Cysteine scanning and modification reveal major differences between BK channels and Kv channels in the inner pore region

Yu Zhou[1], Xiao-Ming Xia, and Christopher J. Lingle

Department of Anesthesiology, Washington University School of Medicine, St. Louis, MO 63110

Edited by Richard W. Aldrich, University of Texas at Austin, Austin, TX, and approved June 6, 2011 (received for review March 15, 2011)

BK channels are regulated by two distinct physiological signals, transmembrane potential and intracellular Ca^{2+}, each acting through independent modular sensor domains. However, despite a presumably central role in the coupling of sensor activation to channel gating, the pore-lining S6 transmembrane segment has not been systematically studied. Here, cysteine substitution and modification studies of the BK S6 point to substantial differences between BK and Kv channels in the structure and function of the S6-lined inner pore. Gating shifts caused by introduction of cysteines define a pattern and direction of free energy changes in BK S6 distinct from *Shaker*. Modification of BK S6 residues identifies pore-facing residues that occur at different linear positions along aligned BK and Kv S6 segments. Periodicity analysis suggests that one factor contributing to these differences may be a disruption of the BK S6 α-helix from the unique diglycine motif at the position of the Kv hinge glycine. State-dependent MTS accessibility reveals that, even in closed states, modification can occur. Furthermore, the inner pore of BK channels is much larger than that of K^+ channels with solved crystal structures. The results suggest caution in the use of Kv channel structures as templates for BK homology models, at least in the pore-gate domain.

cysteine modification | K channels | Slo1 channels

As a unique member of the family of K^+ channels, large conductance, Ca^{2+}-activated K^+ (BK or Slo1) channels are activated in a highly synergistic manner by two distinct physiological signals: depolarization and intracellular Ca^{2+}. To accomplish this, each of the four α-subunits in a functional BK channel is constructed of three modular parts: a voltage-sensing domain composed of S1 to S4 transmembrane segments, a huge cytosolic domain sensing various intracellular ligands, such as Ca^{2+} (1, 2), Mg^{2+} (3), and heme (4, 5), and a pore-gate domain (PGD) formed by S5–pore loop–S6 to allow selective K^+ permeation under the regulation of transmembrane potential and $[Ca^{2+}]_i$ (6–8).

The BK channel shares homology in its membrane-associated domain, including the voltage-sensing domain and PGD, with voltage-dependent K^+ (Kv) channels. Thus, the X-ray crystallographic structures of Kv channels (9, 10) have been widely used as an important template to guide structure–function studies of BK channels (11–13). However, the distant evolutionary relationship between BK and Kv channels (14) raises the possibility that Kv channel structure must be used with caution as a guide to BK channel structure. Sequence alignment (Fig. 1*A*) shows that BK channels and Kv channels differ at two critical positions in their pore-lining S6 transmembrane segments. First, there are two consecutive glycines (i.e., diglycine) at the conserved glycine hinge (15) in BK channels, but only one in the corresponding region of Kv channels. Second, whereas Kv channels share a conserved PXP motif near the cytosolic entrance to the inner pore, in BK channels there is only one proline in this motif. Therefore, variance in the conserved motifs raises the possibility that there may be important differences between BK and Kv channels in the inner pore region that connects the selectivity filter with cytosolic solution (Fig. 1*B*). Consistent with this, functional studies have revealed substantial differences between BK and Kv channels in this region. For example, studies that used cytosolic blockers or sugars of various sizes indicate that the dimension of a BK inner pore is larger than that of a Kv channel (16–19). It has also been proposed that the BK ion permeation gate may reside at the selectivity filter (17, 20, 21) instead of the intracellular entrance of the inner pore, which forms the ion permeation gate in Kv channels (22, 23).

Here we have explored structural differences between BK and Kv channels in the inner pore region. We introduced cysteines throughout the BK S6 and addressed two issues. First, we examined periodicity of gating perturbations introduced by cysteine mutations to determine the secondary structure adopted by BK S6. Second, we examined state-dependent accessibility of introduced cysteines to intracellularly applied water-soluble sulfhydryl reagents to investigate the gating-related conformational change and the geometry of BK inner pore. Based on modifiability of introduced cysteines, likely pore-facing residues in BK channels are rotated relative to those in *Shaker*. Furthermore, based on the pattern of state-dependence of modification, the location of the activation gate in BK channels likely differs from that of Kv channels. Finally, the inner pore of BK channel is much larger than that of Kv channels and other K^+ channels with solved crystal structures.

Results

Periodicity of Energy Perturbation Caused by Cysteine Substitution Reveals α-Helical Composition of BK S6 Transmembrane Segment. To study the structure of BK channel inner pore, we individually mutated 28 S6 residues (from G300 to G327; blue underline in Fig. 1*A*) into a cysteine. The background channel included the C430S mutation, which has been shown to be inert to modification by MTS reagents (24) (Fig. S1). All BK S6 cysteine mutants expressed as functional channels in *Xenopus* oocytes. Almost all cysteine mutations significantly changed the BK gating behavior (Fig. 1 *C* and *E*), with some shifting G–V toward negative potentials and others toward positive potentials. Such gating shifts were not caused by spontaneous disulfide bond formation between introduced cysteines, as the shifts could not be reversed by DTT.

For BK channels, shifts in gating may theoretically arise from effects on voltage-sensing, Ca^{2+}-sensing, or the closed–open (C–O) equilibrium. To confirm that gating shifts arising from S6 mutations reflect primarily effects on the C–O equilibrium, for most constructs, we calculated the free energy difference for a change in Ca^{2+} from 0 to 100 μM ($\Delta\Delta G_{Ca}$). For each mutant, we fit the G–V relationship in 0 or 100 μM Ca^{2+} with the Boltzmann function (Fig. 1*C*) and then calculated the free en-

Author contributions: Y.Z. and C.J.L. designed research; Y.Z. and X.-M.X. performed research; Y.Z. and C.J.L. analyzed data; and Y.Z. and C.J.L. wrote the paper.

The authors declare no conflict of interest.

This article is a PNAS Direct Submission.

[1]To whom correspondence should be addressed. E-mail: zhouy@morpheus.wustl.edu.

This article contains supporting information online at www.pnas.org/lookup/suppl/doi:10.1073/pnas.1104150108/-/DCSupplemental.

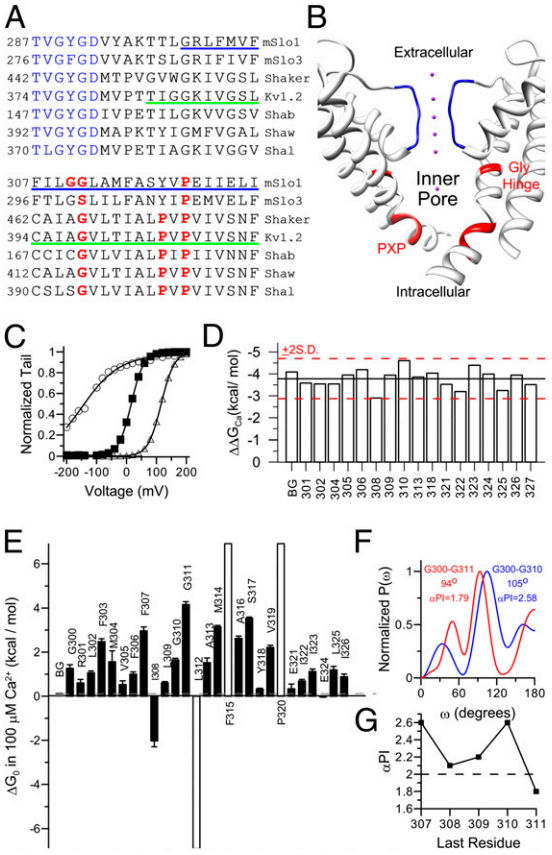

Fig. 1. Periodicity of gating perturbations produced by cysteine mutations reveals α-helical composition of BK S6 transmembrane segment. (*A*) Sequence alignment of the pore-loop and S6 of Slo family channels and Kv family channels. The selectivity filter is colored in blue. The glycine hinge and prolines in the PXP motif are colored in red. The S6 helix in the Kv1.2 crystal structure (Protein Data Bank accession no. 2a79) is marked by a green underline. The cysteine scanning range in BK S6 is marked by a blue underline. (*B*) Side view of Kv 1.2 PGD. For clarity, only two diagonal subunits are displayed. The selectivity filter is colored in blue. The glycine hinge and PXP motif are colored in red. The purple dot is K^+. The structural images in this study were prepared by using the University of California, San Francisco, Chimera system (42). (*C*) G–V relationships of background (filled square), I308C (open circle), and S317C (open triangle) in 100 μM Ca^{2+}. Boltzmann fit results (line) are as follows: z_b = 1.2, V_h = 16.2 mV (background); z_b = 0.5, V_h = −147 mV (I308C); and z_b = 1.2, V_h = 116 mV (S317C). (*D*) The gating energy difference between 0 and 100 μM Ca^{2+} ($\Delta\Delta G_{Ca}$) of background and S6 cysteine mutants. Black line marks the mean value of all $\Delta\Delta G_{Ca}$ in the plot, and red lines mark the mean ±2 SD (*E*) The ΔG_0 of the background (gray) and S6 cysteine mutants (black) in 100 μM $[Ca^{2+}]_i$. The ΔG_0s of three mutants (L312C, F315C, and P320C, unfilled) could not be reliably determined because of the extremely shifted G–Vs of the resulting channels. Thus, these three values were estimated by assuming V_h of 300 mV (F325C and P320C) or −300 mV (L312C) and z_b of 1 (averaged from of the z_bs of background channel and other cysteine mutants). (*F*) Power spectra of $|\Delta\Delta G_0|$ for cysteine mutations from G300C to G310C (blue; peak, 105°; αPI, 2.58) and from G300C to G311C (red; peak, 94°; αPI, 1.79). (*G*) αPIs of BK S6 segments start at 300 and end at different sites from 307 to 311. Dotted line marks the threshold value of 2.

ergy difference between closed and open states at 0 mV (ΔG_0) using the best-fit estimates of half-maximal activation (V_h) and apparent equivalent gating charge (z_b). The $\Delta\Delta G_{Ca}$ was then calculated as the difference in ΔG_0 between gating in 0 and in 100 μM Ca^{2+} (Fig. 1*D*). For all constructs, the $\Delta\Delta G_{Ca}$ was within 2 SD of the overall mean, confirming that S6 segment mutations do not alter Ca^{2+} sensitivity, but mainly change the C–O equilibrium. This justifies comparisons of the mutation-induced gating change at 100 μM Ca^{2+}, a concentration at which the G–V relationships of most mutants can be reliably determined.

To define the strength of the energetic perturbation caused by each mutation, we calculated energy perturbation as the difference in ΔG_0 between mutant and background channels ($\Delta\Delta G_0$) for 27 cysteine mutants in 100 μM Ca^{2+} (Fig. 1*E*). Most mutations increased ΔG_0 and stabilized closed states, whereas three (I308C, L312C, and E324C) reduced ΔG_0 and stabilized open states.

The ΔG_0 map (Fig. 1*E*) reveals a cyclical pattern in which a local maximum gating perturbation appears every three or four residues, consistent with a generally α-helical conformation in BK S6. To examine the S6 periodicity more closely, we used a quantitative periodicity analysis based on a discrete Fourier transform method. This has previously been used to determine the α-helical composition of the transmembrane domain of Kv channels (25, 26). For a typical transmembrane α-helix, the resulting power spectrum of gating perturbation should peak at approximately 105°. Furthermore, the significance of this peak, which is evaluated by a periodicity index (αPI), should be greater than 2 (27, 28). The periodicity analysis could be effectively applied only over S6 positions in which energetic perturbation caused by cysteine introduction could be accurately defined. For the segment from G300 to G311, the power spectrum (Fig. 1*F*, red line) peaks at 94°, near the edge of an α-helical frequency (25). More importantly, the significance of this peak, as defined by αPI, is only 1.79. Thus, the G300–G311 segment fails to exhibit clear α-helical characteristics. On the contrary, the power spectra of shorter stretches preceding G311 showed strong α-helical properties. For example, the power spectrum of gating perturbation in segment G300–G310 (Fig. 1*F*, blue line) peaked at 105° with αPI of 2.58, consistent with an α-helical motif. In fact, the αPIs of S6 N terminus segments are always greater than the threshold value of 2 except when both glycines are included in the analysis (Fig. 1*G*). Although the absence of defined energetic shifts for L312, F315, and P320 preclude application of periodicity analysis to segments following G311, this analysis suggests that the novel diglycine motif may alter or disrupt an otherwise primarily helical structure of BK S6.

State-Dependent Accessibility of Cysteines Substituted in BK S6. We next examined the state-dependent accessibility of S6 cysteines to sulfhydryl reagents applied intracellularly. For comparison with results in *Shaker* channels (23), we chose methanethiosulfonate (MST)–ethyltrimethylammonium(MTSET) as the primary modification reagent. Fig. 2*A* shows an example of MTSET modification of A313C in open states. The inside-out patch was held at 60 mV during the recording. Upon switching from 0-Ca^{2+} control solution into modifying solution containing 100 μM Ca^{2+} and 200 μM MTSET, the current immediately reached a peak and then decayed irreversibly to a steady-state level of approximately 40% of the peak. The decay of the current was fit with a single exponential function to calculate the second order rate constant. Interestingly, the G–V profile of A313C was strongly shifted to negative potentials after MTSET modification. Thus, the open probability of modified channels approached a maximum level at 60 mV even in 0-Ca^{2+} solution (Fig. S2), and the current level showed only a small change between 0 and 100 μM Ca^{2+} (Fig. 2*A*).

The closed-state modification rate was measured in 0 Ca^{2+} solution at −120 mV (Fig. 2*B*, *1*), a condition for which the open probability (P_O) of WT BK channels is lower than 10^{-6} (29). Fig. 2*B*, *2* shows the modification time course of closed A313C by 1 mM MTSET. The modification was much slower but still measurable compared with the open state modification rate. As with the open state, the MTSET modification of A313C in closed states also resulted in tonic opening of the channels.

We systematically examined the state-dependent accessibility to MTSET of cysteines substituted at positions from 309 to 327. Modification rates were determined at 10 sites at which MTSET treatment caused a noticeable irreversible change in current level (Fig. 2*C*). The results reveal several distinct differences

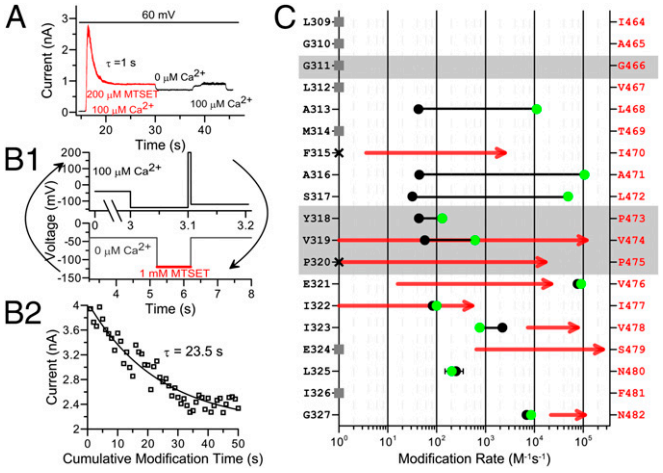

Fig. 2. State-dependent accessibility of S6 cysteines to intracellularly applied MTSET. (*A*) Modification of A313C by 200 μM MTSET in 100 μM $[Ca^{2+}]_i$ with holding potential of 60 mV. After modification, the patch was switched between 0 Ca^{2+} and 100 μM Ca^{2+} to show the tonic opening of modified channels. (*B*) Closed state modification. *1*: Protocol for closed state modification. Patch was first perfused in 100 μM $[Ca^{2+}]_i$. The current level was examined by a brief test pulse of 200 mV at the end of the perfusion. The patch was then washed in control 0 Ca^{2+} for several seconds before being switched into 0-Ca^{2+} solution containing MTS reagent for modification. Membrane potential was held at −120 mV during the modification. After modification, the patch was switched back into the control 0-Ca^{2+} solution to wash out remnant MTS reagent and then switched into 100 μM Ca^{2+} to check current level. This cycle was repeated until current decayed to a steady level. *2*: Time course of closed-state modification of A313C by 1 mM MTSET. The time course is fit with a single exponential function (line). (*C*) Second-order rate constants of MTSET modification are plotted for BK S6 cysteine mutants in the closed (black circles) and open (green circles) states on logarithmic scale. Error bar is displayed only when it is larger than the associated symbol. Seven mutants were not substantially affected by MTSET treatment (gray squares). Two mutants did not generate enough current for tests of modification (black cross). Red lines represent state-dependent modification rates of the corresponding cysteine mutants in *Shaker* channels by intracellularly applied MTSET, with arrowheads indicative of open-state modification rates (23). The glycine and PXP motif are highlighted in gray. The identities of BK (black) and *Shaker* (red) S6 residues are listed on the left and right of the plot, respectively.

between BK and Kv channels in the pattern and rate of S6 MTSET modification. First, although both BK and Kv channels have sites in S6 that exhibit state-dependent modification, the linear position of these sites along S6 relative to the hinge glycine and the PXP motif differs markedly between BK and Kv channels. In BK channels, MTSET modification at three of the 10 MTSET-sensitive sites showed strong state dependence (approximately three orders slower at closed states). These three sites (313, 316, and 317) are all above (i.e., extracellular to) the PXP motif. In contrast, in *Shaker* channels (ref. 23; red lines in Fig. 2*C*), cysteines introduced into sites in or even below (i.e., intracellular to) the PXP motif exhibited strong state dependence on MTSET modification. Second, although the maximum open-state modification rates of BK S6 residues are comparable to those observed in *Shaker* channels, the closed-state modification rates are approximately two orders higher in BK channels (23). Finally, the maximum modification rates of cysteines introduced at 313, 316, and 317 in the BK S6 are comparable to the rate constant of MTSET reaction with free mercaptoethanol [~90,000 $M^{-1}s^{-1}$ (30)], which suggests that the side chains of residues at these sites are exposed to an aqueous environment, presumably the BK inner pore. However, none of the presumed BK pore-facing residues matches the two pore-lining residues (V474,I479) in *Shaker* channels. Based on an alignment of BK S6 to Kv1.2, residues in Kv1.2 that correspond to the BK positions A313, A316, and S317 tend to face away from the aqueous environment (Fig. 3*A*, cyan residues), in contrast to the positions of V474 and I479 in *Shaker* (Fig. 3*A*, red residues). For BK A313, A316, and S317 to point into the ion permeation pathway, we propose that this segment of BK S6 must be rotated relative to the same linear segment in Kv channels.

The prominent shift in gating produced by MTSET modification of A313C is similar to effects of L312C mutation on BK gating (31) (Fig. S2 *A–C*), both of which suggest a preferential stabilization of the open state. We therefore examined the ability of MTSET, 2-aminoethyl MTS (MTSEA), and 2-sulfonatoethyl MTS (MTSES) to produce gating shifts at A313C (Fig. S2*D*) or A317C (Fig. S2*E*). In both positions, irrespective of the net charge on the appended moiety, modification favors the channel open state with particularly strong effects at position A313. The simplest explanation is that MTS modification hinders return of the S6 helix at position A313 to a closed conformation, indicative that position A313 undergoes prominent state-dependent changes in position during gating.

Pore Lining Residues in BK S6. We sought further evidence to support the hypothesis that BK residues at positions 313, 316, and 317 face the inner pore of BK channels. We arranged 15 BK S6 residues below the glycine hinge (A312–I326) in a helical wheel diagram (Fig. 3*B*). In this diagram, three of the four residues resulting in a large positive ΔG_0 in the gating equilibrium lie on the hydrophobic surface of the helix, as indicated by the helical hydrophobic moment (Fig. 3*B*, black arrow), whereas the three sites with maximum modification rates lie on the opposite surface of the helix. This suggests that the former surface is buried in protein, probably participating in protein–protein interactions that are important for defining the C–O equilibrium of BK channels, whereas the latter surface is exposed in the aqueous environment and lines the inner pore of BK channels.

To further confirm that A313C lines the BK pore, we examined interference between MTS modification on A313C and blocking of A313C by tetrabutylammonium (TBA), a well established K^+ channel pore blocker (18). Because TBA is positively charged, we used neutral 2-aminocarbonylethyl MTS (MTSACE) to modify the channels so that any interference between TBA blockade and MTS modification should only result from direct steric hindrance. We first examined if MTSACE modification could change the TBA block. As shown in Fig. 3*C*, modification of A313C by MTSACE modestly reduced the block by 1 mM TBA. We also tested if TBA could protect A313C from being modified by MTSACE. To do this, we first perfused open channels (300 μM Ca^{2+}, 80 mV) in 10 mM TBA and 400 μM MTSACE for 3 s. This treatment only slightly shifted GV leftward (Fig. 3*D*, blue diamond), indicating that most channels were not modified by MTSACE in the presence of TBA. The same patch was then perfused in 400 μM MTSACE for the same duration (3 s) in the same conditions (300 μM Ca^{2+}, 80 mV). All channels were modified and became tonically open in 300 μM Ca^{2+} after this treatment (Fig. 3*D*, red triangle). Thus, TBA protects A313C from being modified by MTSACE. These observations confirm A313C as a pore-lining residue. As residues at 316 and 317 are on the same surface of the helical wheel diagram as residue at 313, these residues should also line the pore. Based strictly on homology mapping onto the structure of Kv1.2, residues A316, S317, and especially A313, would be expected to be buried in the protein (Fig. 3*A*, cyan residues; A313s are highlighted by orange ellipses). Given the evidence that A313, A316, and S317 are pore-facing, this supports the view that the BK S6 helix below the glycine hinge must be rotated relative to that of Kv channels.

MTSET Modification at the Single Channel Level Defines a Lower Limit on the Dimension of the BK Inner Pore. In *Shaker* channels, Cd^{2+} irreversibly inhibits two S6 cysteine mutants (I470C and V474C, corresponding to F315C and V319C in BK, respectively, based on linear alignment) by forming strong coordination with three

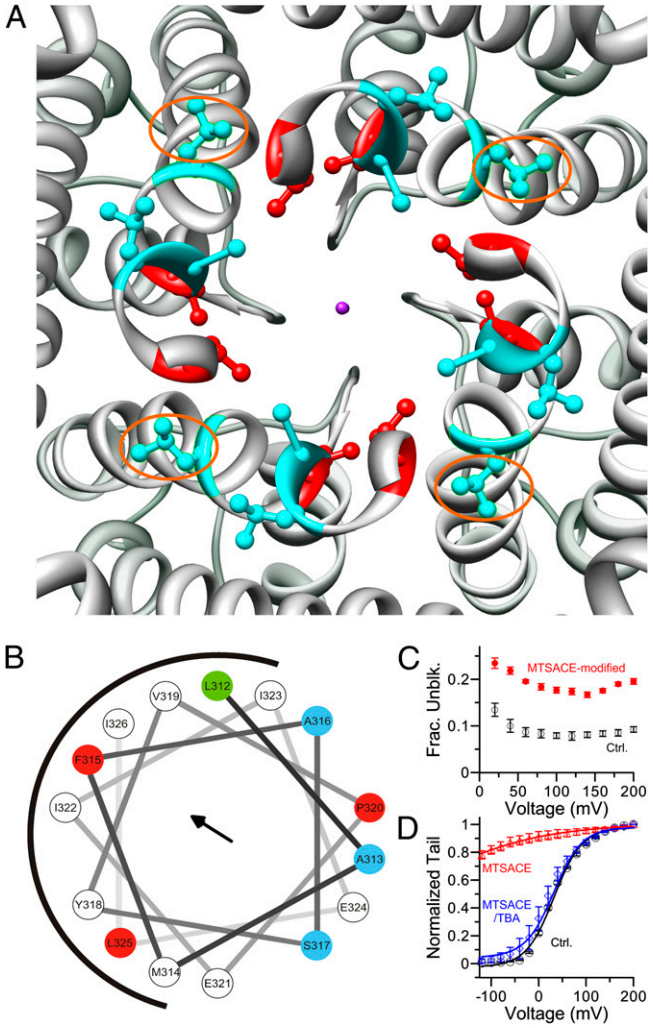

Fig. 3. Pore lining residues in BK channels. (*A*) The S6 pore lining residues of *Shaker* channels (I470, V474; red) and potential pore lining residues of BK channels (A313, A316, S317; cyan) mapped on the crystal structure of Kv 1.2 viewed from intracellular entrance. The purple dot represents K^+. The corresponding residues of BK A313 are marked by orange ellipses. For clarity, S6 below the PXP motif is not rendered. (*B*) Helical wheel diagram of the 15 BK S6 residues below the double glycine hinge (L312–I326). Three residues with maximum MTSET modification rate (A313, A316, S317) are colored in cyan. Three residues (F315, P320, L325) that caused maximum local positive $\Delta\Delta G_0$ when mutated to cysteine are colored in red. Residue L312 that induces the most negative $\Delta\Delta G_0$ when mutated into cysteine is colored in green. The black arrow stands for the helical hydrophobic moment. The diagram was generated online at http://rzlab.ucr.edu/scripts/wheel/wheel.cgi. (*C*) Fractional unblock ratio of A313C by 1 mM TBA before (black open circle) and after (red filled circle) MTSACE modification. (*D*) G–V curves of A313C in 300 μM Ca^{2+} before (black circle), after perfusion in 10 mM TBA and 400 μM MTSACE for 3 s (blue diamond), and after perfusion in 400 μM MTSACE for 3 s (red triangle). To determine the percentage of channels being modified by MTSACE in the presence of TBA, we first fit control GV (black line) and MTSACE-modified (red line) GV with single Boltzmann function. Then, we fit the GV after perfusion in MTSACE and TBA with a double-component Boltzmann function (blue line): $G(V) / G_{max} = (1 - p) / (1 + \exp(z_1F(V_{h1} - V) / R / T)) + p / (1 + \exp[z_1F(V_{h1} - V) / R / T)]$, with only p varying with z_1, V_{h1}, z_2, and V_{h2} being fixed, with the values determined from previous fit results. This gave a *P* value of 0.05, suggesting that only 5% of the channels were modified by MTSACE in the presence of TBA.

or four cysteines individually introduced at these pore lining sites (23). This coordination by Cd^{2+} defines a diameter in *Shaker* of approximately 8 to 9 Å separating diagonal cysteines (32). In BK channels, however, we observed no irreversible inhibition produced by Cd^{2+} treatment at any of the S6-substituted cysteine mutants. This indicates that the dimension of the BK inner pore is sufficiently larger than that of *Shaker* channels such that Cd^{2+} cannot be multivalently coordinated by three to four cysteines at any of the pore lining sites. By using the three pore-lining sites A313, A316, and S317, we next examined MTSET modification at the single-channel level to obtain information on the geometry of the BK inner pore. For A313C, we found that there was one intermediate level between the initial and final conducting level during MTSET modification (Fig. 4*A*). This requires that at least two of the four cysteines introduced at 313 can be simultaneously modified, but that even modification of two cysteines is not sufficient to fully block channel conductance. Two modification steps were also observed for S317C (Fig. 4*C*). For A316C, MTSET modification completely eliminated single-channel current, and there was no intermediate conducting level (Fig. 4*B*). However, this mutant was still conductive after it was modified by a smaller neutral MTS reagent, MTSACE (Fig. S3). Thus, the complete inhibition of A316C by MTSET modification likely results from occlusion of the ion permeation pathway but not from an extreme gating shift. This also suggests that a BK channel can be modified only once by MTSET at the level of 316.

We attempted to define a minimum estimate of the size of a pore that would accommodate at least two MTSET head groups (~3 Å in radius) and one hydrated potassium ion (3~4 Å in radius; Fig. 5*A*). We assumed an absolute minimum extension of MTSET from the sides of the S6 helix. With this assumption, the radius of the BK inner pore at the level of A313 or S317 should not be less than 7.3 Å. Considering that both MTSET and the K^+ ion are positively charged and that MTSET is likely to protrude considerably into the pore, this value is likely to substantially underestimate the true dimension of the BK inner pore at position A313. Even so, this value is much larger than any of the K^+ channels with solved crystal structures (Fig. 5*B*). However, at the level of A316, the BK channel does not allow permeation of K^+ after modification by one MTSET. This suggests that the radius at this level may be narrower than that at 313 or 317. However, we found that A313C could be modified by a large MTS reagent, Texas red–MTSEA (TR-MTSEA; Fig. S4). As the distance between the head group of TR-MTSEA and its sulfhydryl-reactive group is less than the pitch of an α-helix (i.e., the vertical distance between consecutive turns of the helix) (33), it requires that the large head group (6.5 Å in radius) of TR-MTSEA must pass by A316 to modify A313C. Thus, the radius of the BK inner pore at the level of 316 should be no less than 6.5 Å. Therefore, the dimension of the BK inner pore is much larger than that of all K^+ channels for which structural information is so far available.

Discussion

We have performed cysteine scanning mutagenesis and state-dependent cysteine accessibility studies to gain structural and functional insight into the BK inner pore lined by the S6 transmembrane segment. The results reveal several important differences between BK and Kv channels in this region.

Our analysis of gating equilibria suggests that BK and Kv channels differ in the role of S6 residues in defining energetics of channel gating. In particular, introduction of Ala (34, 35) or Cys (23) into *Shaker* S6 positions generally promotes channel opening, whereas most Cys mutations in BK S6 favor closure. Furthermore, the energetically most important residues in *Shaker* do not align well with those in BK, except for perhaps the second P in the PXP motif. Superficially, such differences suggest that the interactions experienced by S6 residues between C and O states must differ markedly between BK and Kv channels. Perhaps correlated with this, our MTS modification experiments show that the S6 pore lining residues in BK channels and *Shaker* channels do not lie on the same surface when mapped onto the Kv1.2 structure (Fig. 3*A*). For example, to align the side chains of the inner most pore-lining residues in BK and Kv channels—i.e., to bring the side chain of A313 into alignment with that of I470

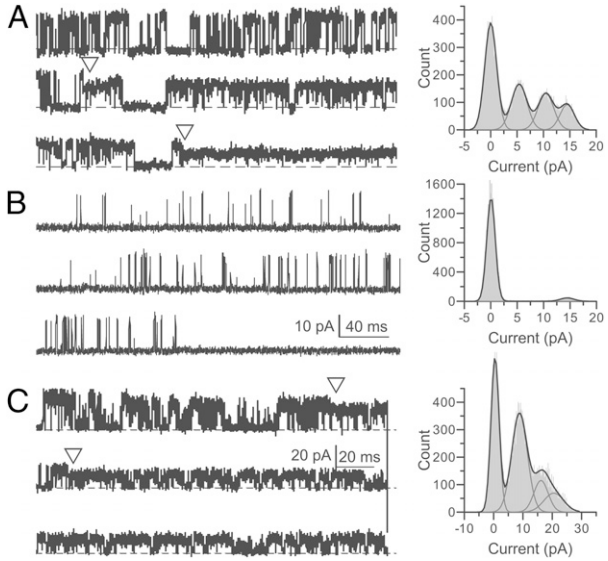

Fig. 4. Modification of pore-lining cysteines by MTSET at the single channel level. Opening is upward. (*A*) *Left*: Single channel current of A313C perfused in 80 μM MTSET and 300 μM Ca^{2+} at 60 mV. Triangles mark the beginning and the of the intermediate current level. *Right*: All-point histogram of this recording. The single channel conductances of three conducting levels are 241, 173, and 90 pS, respectively. (*B*) *Left*: Single-channel current of A316C perfused in 20 μM MTSET and 300 μM Ca^{2+} at 60 mV. *Right*: All-point histogram of this recording. The single-channel conductance of the only conducting level is 233 pS. *A* and *B* have the same scale bar. (*C*) *Left*: Single-channel current of S317C perfused in 20 μM MTSET and 300 μM Ca^{2+} at 90 mV. Triangles mark the beginning and end of the intermediate current level. *Right*: All-point histogram of this recording. The single-channel conductances of the three conducting levels are 233, 180, and 100 pS, respectively. No additional reduction of current was observed with ongoing perfusion. In *A* and *C*, segments before the first triangle are from unmodified channels.

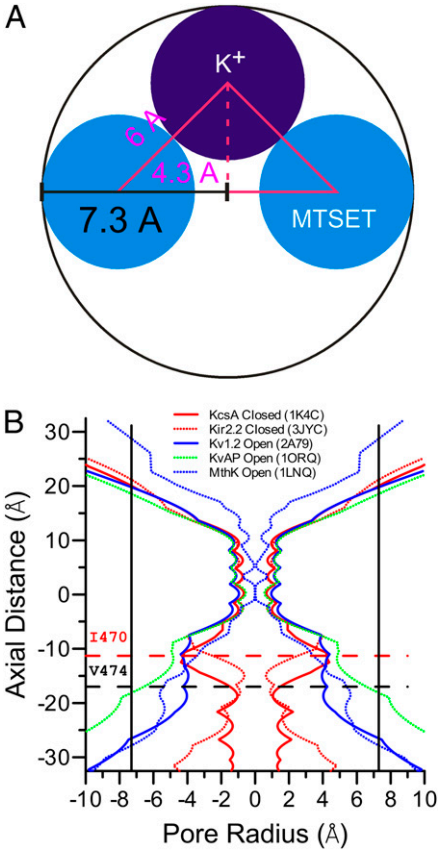

Fig. 5. The BK inner pore is much broader than that of many other K^+ channels. (*A*) Estimation of the minimal radius of BK pore at positions that allow two independent modifications by MTSET, A313C and S317A, based on the size of MTSET (3 Å in radius, blue sphere) and hydrated K^+ (3 Å in radius, purple sphere). (*B*) Radius profiles of various K^+ channels were calculated from their crystal structures by using the program HOLE (43). The horizontal dotted lines mark the levels of *Shaker* I470 (red) and V474 (black), respectively. The vertical lines mark the minimal radius of 7.3 Å at the level of 313 or 317 in the BK inner pore.

in the Kv1.2 structure—a clockwise rotation of approximately 86° (viewed from the intracellular entrance of the pore) would be required. Furthermore, the modification of BK pore lining cysteines by MTSET at the single-channel level indicates that the BK inner pore is much larger than those of many K^+ channels.

Together, the energetic, accessibility, and size differences require that the inner pore structures of BK and Kv channels differ markedly. Although the results do not define a BK inner pore structure, one might imagine a number of ways in which the differences we observe might be brought about. From the simple assumption that the larger inner pore dimension arises solely from expansion around the pore axis, the differences in accessibility might suggest a rotation in BK S6 relative to Kv. Although this may be the case, the larger BK inner pore dimension may also be associated with substantial tilt in S6 relative to Kv channels that might also be expected to impact on residue accessibility.

Our examination of the periodicity within BK S6 suggests one possible factor that might contribute to such differences. Namely, the BK S6 α-helix may be in some way disrupted by the two consecutive glycines (Fig. 1 *E* and *F*), whereas, in the Kv 1.2 crystal structure, the S6 helices seem to be continuous around the glycine hinge (9). The importance of the diglycine motif in defining BK S6 orientation is also supported by the absolute dependence of paxilline block on the presence of G311 (36). However, other factors may also contribute to a different orientation between BK and Kv S6, perhaps originating at the demarcation between S6 and the P-loop. Irrespective of its origins, a difference in BK and Kv S6 orientation would naturally predict that interactions of S6 residues with other S6 residues or other elements of the PGD would differ between *Shaker* and BK. It has been proposed that the interaction between S6 and other regions in the protein, such as the S4–S5 linker (37), is critical for K^+ channel gating. The properties of BK S6 seem likely to require substantially different potential interactions than those inferred from the Kv1.2 structure. It is important to take this into account when the structure of Kv channels is used as a guide for study of BK channel structure/function.

The present results also support for the idea that the location of the BK ion permeation gate is not formed at the same location as that of a Kv channel. In Kv channels, the ion permeation gate is formed just intracellular to the PXP motif that forms a tight steric exclusion when it has closed (22, 23). Thus, strong state dependence of modification by intracellularly applied MTSET was observed on cysteines introduced into sites in the PXP motif (22). In contrast, BK S6 cysteine mutants in the segment cytosolic to the BK YVP motif show little state-dependent modification. All sites showing strong state dependence of MTSET modification in BK S6 are extracellular to the YVP motif (Fig. 2*C*). Thus, even if the slower closed-state modification rate observed at positions 313, 316, and 317 in BK channels was caused by narrowing between the inner pore and the cytosolic milieu, this constriction should reside more extracellularly along the pore than that of the Kv channels. It should also be noted that the closed-state modification rates at the three BK pore-lining sites are approximately two orders higher than that of the *Shaker* channels (23). These rates are even several fold higher than that of closed cyclic nucleotide-gated channels (38), the ion perme-

ation gate of which has been determined to be in the selectivity filter region (38, 39). In accord with previous results that small molecules such as quaternary ammonium blockers may pass in and out of the BK inner pore in both open and closed states (17, 20), this observation suggests that any constriction at the cytosolic end of BK S6 does not prevent access of molecules to the inner pore and thus is unlikely to form an ion permeation gate.

The differences defined here also suggest that the motion of S6 during channel gating might be quite different between BK and Kv channels. In the *Shaker* channel, it has been suggested that opening of the gate is expected to be accomplished by swiveling the lower half of the S6 below the PXP motif (32, 40), with only modest changes in dimension at the position of V474C within the *Shaker* PVP motif (23, 32). Although gating shifts reported for V474 mutation may somewhat contradict the idea that V474 changes little during gating (34, 35), it is the case that *Shaker* S6 positions with the strongest energetic effects on gating extend largely from V474 down to perhaps N482. *Shaker* residues that follow the hinge glycine have less impact on gating. In contrast, for BK channels, our observations suggest that there is a major conformational change or rotation that involves residues that closely follow the BK diglycine motif. In particular, mutation of L312 and F315 each produce profound shifts in gating (31), whereas the corresponding residues in *Shaker* following the hinge glycine have minimal effect. Furthermore, in the same short segment of S6, modification of A313C by MTSET (and other MTS reagents) results in essentially tonic activation of the channels (Fig. 2*A* and Fig. S2), very similar to the effect of introduction of cysteine at the adjacent position L312 (31). One speculation is the gating-associated conformational change in BK S6 includes a rotation of the helix. The presence of an MTS moiety may hinder the ability of A313C and adjacent residues to rotate back into the closed conformation, thus stabilizing the channels in the open conformation. If this is true, activation of the BK channel is more like that of ligand-gated cyclic nucleotide-gated channel, in which rotational movement of S6 is required for gating (41). In addition, the strong state-dependent modification of BK pore-lining cysteines by MTSET could be at least partly caused by such rotation.

In summary, despite extensive conservation between BK and Kv channels in their transmembrane domains, the present work highlights major differences between BK and Kv channels in the pore-lining S6 transmembrane segment and points out that caution is warranted in regards to the use of homology models as structural surrogates for phylogenetically distant proteins.

Materials and Methods

Mutagenesis and Channel Expression. Mutants were prepared as described before (2). cRNA was injected in stage IV *Xenopus* oocytes. Recording was performed 2 to 7 d after injection.

Electrophysiology and Data Analysis. Electrophysiology and data analysis are described in *SI Materials and Methods*.

Chemicals. MTS reagents were obtained from Toronto Research Chemicals. TBA was obtained from Alfa Aesar. KOH solution (1N) was obtained from Fisher Scientific. All other chemicals were purchased from Sigma-Aldrich.

ACKNOWLEDGMENTS. We thank Joe Henry Steinbach for insightful comments and Jennifer Jones for assistance with injection and maintenance of oocytes. This work was supported by National Institute of General Medical Sciences/National Institutes of Health Grant GM066215 (to C.J.L.).

1. Schreiber M, Salkoff L (1997) A novel calcium-sensing domain in the BK channel. *Biophys J* 73:1355–1363.
2. Xia XM, Zeng X, Lingle CJ (2002) Multiple regulatory sites in large-conductance calcium-activated potassium channels. *Nature* 418:880–884.
3. Shi J, et al. (2002) Mechanism of magnesium activation of calcium-activated potassium channels. *Nature* 418:876–880.
4. Tang XD, et al. (2003) Haem can bind to and inhibit mammalian calcium-dependent Slo1 BK channels. *Nature* 425:531–535.
5. Horrigan FT, Heinemann SH, Hoshi T (2005) Heme regulates allosteric activation of the Slo1 BK channel. *J Gen Physiol* 126:7–21.
6. Lingle CJ (2007) Gating rings formed by RCK domains: Keys to gate opening. *J Gen Physiol* 129:101–107.
7. Magleby KL (2003) Gating mechanism of BK (Slo1) channels: so near, yet so far. *J Gen Physiol* 121:81–96.
8. Salkoff L, Butler A, Ferreira G, Santi C, Wei A (2006) High-conductance potassium channels of the SLO family. *Nat Rev Neurosci* 7:921–931.
9. Long SB, Campbell EB, Mackinnon R (2005) Crystal structure of a mammalian voltage-dependent Shaker family K+ channel. *Science* 309:897–903.
10. Long SB, Tao X, Campbell EB, MacKinnon R (2007) Atomic structure of a voltage-dependent K+ channel in a lipid membrane-like environment. *Nature* 450:376–382.
11. Ma Z, Lou XJ, Horrigan FT (2006) Role of charged residues in the S1-S4 voltage sensor of BK channels. *J Gen Physiol* 127:309–328.
12. Yang H, et al. (2008) Activation of Slo1 BK channels by Mg2+ coordinated between the voltage sensor and RCK1 domains. *Nat Struct Mol Biol* 15:1152–1159.
13. Liu G, et al. (2008) Position and role of the BK channel alpha subunit S0 helix inferred from disulfide crosslinking. *J Gen Physiol* 131:537–548.
14. Yu FH, Catterall WA (2004) The VGL-chanome: A protein superfamily specialized for electrical signaling and ionic homeostasis. *Sci STKE* 2004:re15.
15. Magidovich E, Yifrach O (2004) Conserved gating hinge in ligand- and voltage-dependent K+ channels. *Biochemistry* 43:13242–13247.
16. Li W, Aldrich RW (2006) State-dependent BLOCK of BK channels by synthesized shaker ball peptides. *J Gen Physiol* 128:423–441.
17. Wilkens CM, Aldrich RW (2006) State-independent block of BK channels by an intracellular quaternary ammonium. *J Gen Physiol* 128:347–364.
18. Li W, Aldrich RW (2004) Unique inner pore properties of BK channels revealed by quaternary ammonium block. *J Gen Physiol* 124:43–57.
19. Brelidze TI, Magleby KL (2005) Probing the geometry of the inner vestibule of BK channels with sugars. *J Gen Physiol* 126:105–121.
20. Tang QY, Zeng XH, Lingle CJ (2009) Closed-channel block of BK potassium channels by bbTBA requires partial activation. *J Gen Physiol* 134:409–436.
21. Piskorowski RA, Aldrich RW (2006) Relationship between pore occupancy and gating in BK potassium channels. *J Gen Physiol* 127:557–576.
22. del Camino D, Yellen G (2001) Tight steric closure at the intracellular activation gate of a voltage-gated K(+) channel. *Neuron* 32:649–656.
23. Liu Y, Holmgren M, Jurman ME, Yellen G (1997) Gated access to the pore of a voltage-dependent K+ channel. *Neuron* 19:175–184.
24. Zhang G, Horrigan FT (2005) Cysteine modification alters voltage- and Ca(2+)-dependent gating of large conductance (BK) potassium channels. *J Gen Physiol* 125:213–236.
25. Li-Smerin Y, Hackos DH, Swartz KJ (2000) Alpha-helical structural elements within the voltage-sensing domains of a K(+) channel. *J Gen Physiol* 115:33–50.
26. Li-Smerin Y, Swartz KJ (2001) Helical structure of the COOH terminus of S3 and its contribution to the gating modifier toxin receptor in voltage-gated ion channels. *J Gen Physiol* 117:205–218.
27. Cornette JL, et al. (1987) Hydrophobicity scales and computational techniques for detecting amphipathic structures in proteins. *J Mol Biol* 195:659–685.
28. Komiya H, Yeates TO, Rees DC, Allen JP, Feher G (1988) Structure of the reaction center from Rhodobacter sphaeroides R-26 and 2.4.1: Symmetry relations and sequence comparisons between different species. *Proc Natl Acad Sci USA* 85: 9012–9016.
29. Horrigan FT, Cui J, Aldrich RW (1999) Allosteric voltage gating of potassium channels I. Mslo ionic currents in the absence of Ca(2+). *J Gen Physiol* 114:277–304.
30. Stauffer DA, Karlin A (1994) Electrostatic potential of the acetylcholine binding sites in the nicotinic receptor probed by reactions of binding-site cysteines with charged methanethiosulfonates. *Biochemistry* 33:6840–6849.
31. Wu Y, et al. (2009) Intersubunit coupling in the pore of BK channels. *J Biol Chem* 284: 23353–23363.
32. Webster SM, Del Camino D, Dekker JP, Yellen G (2004) Intracellular gate opening in Shaker K+ channels defined by high-affinity metal bridges. *Nature* 428:864–868.
33. Anonymous (2010) Open for business. *Nat Commun* 1:1.
34. Yifrach O, MacKinnon R (2002) Energetics of pore opening in a voltage-gated K(+) channel. *Cell* 111:231–239.
35. Hackos DH, Chang TH, Swartz KJ (2002) Scanning the intracellular S6 activation gate in the shaker K+ channel. *J Gen Physiol* 119:521–532.
36. Zhou Y, Tang QY, Xia XM, Lingle CJ (2010) Glycine311, a determinant of paxilline block in BK channels: A novel bend in the BK S6 helix. *J Gen Physiol* 135:481–494.
37. Long SB, Campbell EB, Mackinnon R (2005) Voltage sensor of Kv1.2: Structural basis of electromechanical coupling. *Science* 309:903–908.
38. Flynn GE, Zagotta WN (2001) Conformational changes in S6 coupled to the opening of cyclic nucleotide-gated channels. *Neuron* 30:689–698.
39. Contreras JE, Srikumar D, Holmgren M (2008) Gating at the selectivity filter in cyclic nucleotide-gated channels. *Proc Natl Acad Sci USA* 105:3310–3314.
40. del Camino D, Holmgren M, Liu Y, Yellen G (2000) Blocker protection in the pore of a voltage-gated K+ channel and its structural implications. *Nature* 403:321–325.
41. Johnson JP, Jr., Zagotta WN (2001) Rotational movement during cyclic nucleotide-gated channel opening. *Nature* 412:917–921.
42. Pettersen EF, et al. (2004) UCSF Chimera—a visualization system for exploratory research and analysis. *J Comput Chem* 25:1605–1612.
43. Smart OS, Neduvelil JG, Wang X, Wallace BA, Sansom MS (1996) HOLE: A program for the analysis of the pore dimensions of ion channel structural models. *J Mol Graph* 14: 354–360, 376.